# Costs and constraints from time-delayed feedback in small gene regulatory motifs

**Andreas Grönlund[a], Per Lötstedt[b], and Johan Elf[c,1]**

[a]Department of Mathematics, Uppsala University, SE-751 06 Uppsala, Sweden; [b]Division of Scientific Computing, Department of Information Technology, Uppsala University, SE-751 05 Uppsala, Sweden; and [c]Department for Cell and Molecular Biology, Uppsala University, SE-751 24 Uppsala, Sweden.

Edited by Peter G Wolynes, University of California, San Diego, La Jolla, CA, and approved March 16, 2010 (received for review November 17, 2009)

**The multistep character of transcription, translation, and protein modification inevitably leads to time delays between sensing gene regulatory signals and responding with changed concentrations of functional proteins. However, the interplay between the time-delayed and the stochastic nature of gene regulation has been poorly investigated. Here we present an extension of the linear noise approximation which makes it possible to estimate second moments—variances and covariances—of fluctuations around stationary states in time-delayed systems. The usefulness of the method is exemplified by analyzing two ubiquitous regulatory motifs. In the first system, we show that there is an optimal combination of transcriptional repression and direct product inhibition in determining the activity of an enzyme system. In particular, we demonstrate that direct product inhibition is necessary to avoid deleterious fluctuations in a system when the gene regulatory response is delayed. The second system is an anabolic motif where the substrate fluxes are balanced by time-delayed regulation responding to the substrate concentrations. The extended linear noise approximation makes it possible to show analytically that increased association rate between the substrates leads to a lower product flux because of increasing unbalance in substrate pools.**

biochemical networks | intrinsic noise

The wiring and dynamics of intracellular biochemical networks govern the cells' functions. It is however not clear, a priori, at which level of detail the interactions need to be modeled to capture the relevant properties of the systems, that is, the properties that contribute to the evolutionary fitness of the organism. In some cases, chemical fluctuations should be considered (1). In other cases, average properties do not depend on the fluctuations and a deterministic mean-field treatment suffices (2). In some cases, spatial considerations are necessary, but often diffusion is fast compared to the timescale of the reactions and there is no significant spatial correlation between reaction events. Sometimes genome scale networks are considered when trying to map the genotype to the phenotype (3), but often it is meaningful to analyze properties of commonly reoccurring subsystems (motifs) in isolation (4). Even for small motifs with a limited number of components, it is often necessary to further reduce the state description to capture the relevant kinetics in a comprehensible model. For example, it is often motivated to replace all the individual states an RNA polymerase goes though when it transcribes a whole gene with a single state. However, the time from initiating to completing transcription is in this case not exponentially distributed as it would be for a single-step process; instead, it may have a relatively narrow distribution that is better approximated by a fixed time delay. The framework for analyzing time-delayed deterministic systems with ordinary differential equations (ODEs) is well worked out (5). However, when we also need to consider the stochastic aspects of chemical reactions there are essentially no straightforward methods for analysis and one often has to resort to Monte Carlo simulation (6–8). In this paper, we will introduce a method for considering the combined effects of noise and time-delayed regulation in the analysis of small kinetic motifs. To put the analysis into biological context, we specifically study two small, but ubiquitous, systems: (*i*) feedback controlled enzymatic activity (CEA) and (*ii*) flux-coupled dimerization (FCD).

## Models

**Feedback Controlled Enzymatic Activity.** This motif is part of a linear enzymatic cascade where an enzyme $E$ synthesizes a product $X$ that is used as a substrate for an other enzyme $E_2$. When $E$ tries to keep $E_2$ close to saturation, the consumption of $X$ is close to zero order and there will be very large stochastic fluctuations in the concentration of $X$ unless the activity of $E$ is carefully regulated (9). Such regulation is commonly mediated through the concentration of $X$ that reduces its own synthesis by direct product inhibition of $E$ and through indirect transcriptional repression of the expression of $E$ through an allosterically activated repressor (10). The motif is characterized by the following reactions:

$$S \xrightarrow{\frac{Ek_{\mathrm{cat}}}{1+(x/K_I)}} X \qquad X \xrightarrow{\frac{V_{\max}}{1+(K_M/x)}} P$$

$$\varnothing \xrightarrow{\frac{\alpha}{1+(x_\tau/K_R)^n}} E \qquad E \xrightarrow{\beta E} \varnothing$$

where the synthesis rate of $E$ at time $t$ is regulated by the concentration of $X$ at time $t-\tau$, i.e., $x_\tau$. It is assumed that the concentration of substrate for $E$ as well as the concentration of $E_2$ are constant. To keep things relatively simple, we will further assume that the dynamics in $E$ and $X$ are slower than the timescale for equilibration binding of enzymes with substrates and products as well as that of repressor binding kinetics.

***Control accuracy.*** The task for the control system is to maintain a stable concentration even when $E_2$ is near saturation $x > K_M$ and large zero-order fluctuations are expected for a nonregulated system (9). For this reason, we simply define the control accuracy of the feedback regulation as the inverse Fano factor

$$\Psi_{\mathrm{CEA}} = \frac{1}{\mathcal{F}_X} = \frac{\langle X \rangle}{\sigma_X^2}, \qquad [1]$$

which will have a low value ($\ll 1$) if $x$ fluctuates wildly. If the fluctuations display Poissonian statistics, $\Psi = 1$. Therefore, $\Psi \geq 1$ is a measure of an efficient regulation and thus a good control accuracy.

***Throughput.*** When feedback regulation is used to reduce noise by direct product inhibition, the activity of the enzymes are

Author contributions: A.G., P.L., and J.E. designed research, performed research, and wrote the paper.

The authors declare no conflict of interest.

This article is a PNAS Direct Submission.

[1]To whom correspondence should be addressed. E-mail: johan.elf@icm.uu.se.

This article contains supporting information online at www.pnas.org/lookup/suppl/doi:10.1073/pnas.0913317107/-/DCSupplemental.

compromised, which infers a cost of the regulation in terms of reduced flux. The throughput is therefore defined as the flux through the system compared to the maximal flux ($=Ek_{\mathrm{cat}}$),

$$\Phi_{\mathrm{CEA}} = \left\langle \frac{Ek_{\mathrm{cat}}}{1+X/K_I} / Ek_{\mathrm{cat}} \right\rangle = \left\langle \frac{1}{1+X/K_I} \right\rangle. \qquad [2]$$

**Flux-Coupled Dimerization.** The second motif is a flux-coupled anabolic reaction system, where two species, $X$ and $Y$, are independently synthesized and but stoichometrically consumed in a two-substrate reaction (1, 9), i.e.,

$$\begin{array}{ccccc} \varnothing & \overset{\alpha/(1+(x_\tau/K_R)^n)}{\rightarrow} & X & \overset{\beta x}{\rightarrow} & \varnothing \\ \varnothing & \overset{\alpha/(1+(y_\tau/K_R)^n)}{\rightarrow} & Y & \overset{\beta y}{\rightarrow} & \varnothing \\ & X+Y & \overset{\epsilon xy}{\rightarrow} & P & \end{array}$$

Here, $X$ and $Y$ can be two metabolites in an anabolic pathway, an mRNA (11) and its antisense RNA (12, 13), two proteins that form a heterodimer, etc. For simplicity, the two-substrate reaction is taken to be a simple second-order association process. However, many types of unsaturated catalyzed reactions would give the system the same properties as long as the reactions are driven far from equilibrium such that they can be considered irreversible. The major consumption pathway of $X$ and $Y$ are through the dimerization reaction at rate $\epsilon xy$ but there are also nonproductive losses through first-order degradation or dilution at rate β. In order to balance the synthesis of $X$ and $Y$, the synthesis fluxes are feedback inhibited in response to the respective $X$ and $Y$ pool. For example, if $X$ and $Y$ are two amino acids that are synthesized by a cascade of biosynthetic enzymes and consumed in protein synthesis, their synthesis will typically be inhibited at an early state of the enzymatic cascade by the end product, the amino acid itself (10). Or, if $X$ and $Y$ are ribosomal proteins, they will feed back on their own translation when more is produced than what can be used in ribosomal assembly (14). In either case, there will be a time delay between the moment when the control system senses the change in the pool and when the synthesis flux is changed. The feedback is here simply modeled with sigmoidal repression function with sensitivity $n$ responding to the time-delayed signals. The current synthesis rates of $X$ and $Y$ are thus regulated by respective concentrations $x_\tau$ and $y_\tau$ at time $t-\tau$. The motif and the parameters connected to the different processes are illustrated in Fig. 1.

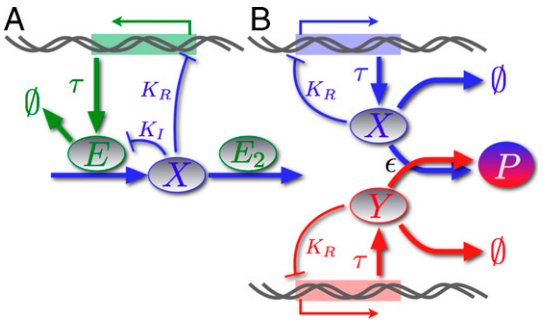


**Fig. 1.** (*A*) Feedback controlled enzymatic activity, the CEA motif. The enzyme $E$ is produced in a multistep process covering $\tau$ s. The synthesis of $E$ is transcriptionally repressed at high concentrations of its product $X$, which also inhibits the enzyme's activity directly. (*B*) Flux-coupled dimerization, the FCD motif. $X$ and $Y$ are produced in multistep processes covering $\tau$ s. The synthesis of each molecule is negative feedback inhibited to balance their concentration. The consumption is stoichiometrically coupled through the making of $P$.

***Control accuracy.*** The goal of the feedback regulation is to balance the pools such that the investment in substrates $X$ and $Y$ is used for production of $P$ instead of losing them through the decay pathways. Therefore, the control accuracy is given by the ratio of the actual product flux $\epsilon\langle XY\rangle$ and the maximally possible flux ($=\epsilon\langle X\rangle\langle Y\rangle$) given a fixed total investment in $X$ and $Y$ ($=\langle X\rangle+\langle Y\rangle$).

$$\Psi_{\mathrm{FCD}} = \frac{\epsilon\langle XY\rangle}{\epsilon\langle X\rangle\langle Y\rangle} = \frac{\langle XY\rangle}{\langle X\rangle\langle Y\rangle} \qquad [3]$$

Here, $0 < \Psi < 1$, where 1 corresponds to a perfect balance between the $X$ and $Y$ pools.

***Throughput.*** The feedback control of the FCD motif can be tuned to maintain a balanced concentration of the two components at the cost of limited throughput, which is defined here as the product flux divided by the maximal product flux

$$\Phi_{\mathrm{FCD}} = \frac{\epsilon\langle XY\rangle}{\alpha} \qquad [4]$$

## Methods and Results

Our starting point in the analysis is the chemical master equation (CME) (15), which describes the probability that the system is in a particular state at a certain point in time. The CME can be expanded in powers of the system volume (Ω). The first-order expansion results in a set of ODEs describing the average rates of change in the macroscopic limit, the reaction rate equations. They accurately describe the kinetics in macroscopic well-stirred systems without time delays (15). However, if the reaction rates depend nonlinearly on the state of the system, the deterministic mean-field solution does not necessarily give an accurate description of the average behavior in a system of limited volume. Any conclusion drawn from the macroscopic analysis may therefore need to be justified in terms of a more detailed description that considers the stochastic, discrete nature of chemical reactions. We will therefore start the analysis of the motifs with a description of their expected macroscopic properties and then complement this analysis with a characterization of their stochastic properties that will be necessary to evaluate the control accuracy of the feedback systems.

Throughout the text, the Hill coefficient $n$ describing the cooperative feedback is a positive number in the theoretical parts but the discussion and the explicit calculations for the figures are restricted to $n = 2$.

**Mean-Field Dynamics for Time-Delayed Feedback.** The macroscopic dynamics of the CEA motif are given by two ODEs. They can be written in nondimensional form by rescaling the concentrations $\hat{x} = x/K_M$, $\hat{E} = Ek_{\mathrm{cat}}/K_M\beta$, and time $\hat{t} = \beta t$. This leaves us with four parameters $\sigma = (\alpha k_{\mathrm{cat}}/\beta)\cdot(1/K_M\beta)$, $\hat{K}_R = K_R/K_M$, $\hat{K}_I = K_I/K_M$, and $\hat{V}_{\max} = V_{\max}/K_M\beta$. Thus concentrations of $x$ are given in number of $K_M$, time is given terms of the decay time of $E$, and the units of $E$ are defined such that $\hat{E} = 1$ makes a concentration of $K_M$ during its lifetime $(1/\beta)$. The ODEs with the rescaled variables and parameters are

$$\frac{d\hat{E}}{d\hat{t}} = \frac{\sigma}{1+(\hat{x}_\tau/\hat{K}_R)^n} - \hat{E} \qquad \frac{d\hat{x}}{d\hat{t}} = \frac{\hat{E}}{1+\hat{x}/\hat{K}_I} - \frac{\hat{V}_{\max}}{1+1/\hat{x}}. \qquad [5]$$

Because we want $E_2$ near saturation, $\hat{x} = x/K_M > 1$, the stationary solution $\hat{x}_0$ of Eq. **5** should satisfy $\hat{x}_0 > 1$. We thus fixate $\hat{x}_0 = \hat{\xi} > 1$, or equivalently, $x_0 = \xi > K_M$. By doing so, we can compute σ from the stationary solution for each combination of $\hat{K}_R$, $\hat{K}_I$, and $\hat{V}_{\max}$. The dynamics of the FCD motif can likewise

be written in nondimensional form by the scaling $\hat{x} = x/K_R$, $\hat{y} = y/K_R$, and time as $\beta, \hat{t} = \beta t$. We get the rescaled synthesis rate $\sigma = \alpha/K_R\beta$ and association rate $\kappa = \epsilon K_R/\beta$ and the ODEs are

$$\frac{d\hat{x}}{d\hat{t}} = \frac{\sigma}{1+\hat{x}_\tau^n} - \kappa\hat{x}\hat{y} - \hat{x} \qquad \frac{d\hat{y}}{d\hat{t}} = \frac{\sigma}{1+\hat{y}_\tau^n} - \kappa\hat{x}\hat{y} - \hat{y}. \qquad [6]$$

In *SI Text* the stability of the time-delayed motifs is analyzed (5). In this analysis the eigenvalues of the Jacobians of Eqs. **5** and **6** dictate the time evolution of the system after a small perturbation from the fixed points. With no delay ($\tau = 0$), both motifs display one stable fixed point (having real negative eigenvalues of the Jacobians) for all parameter combinations. If, on the other hand, $\tau > 0$, both motifs can display sustained oscillations (having imaginary eigenvalues with zero real part of the Jacobians) if the delay is sufficiently long. From the fixed point analysis (*SI Text*), we plot in Fig. 2 the bifurcation diagram to show the parameter regions with oscillations. The mathematical criteria for oscillations are given in the *SI Text*. Here we simply state that the product $X$ for the CEA motif can oscillate even for short time delays ($\tau \approx 1/\beta$) if transcriptional feedback is strong ($K_R/K_M < 1$) and direct product inhibition is weak ($K_I/K_M > 1$). The FCD motif $X$ and $Y$ will display anticorrelated oscillations for shorter time delays when the turnover of the pools increases in relation to the feedback inhibition constant, i.e. if $\alpha/K_R\beta$ is large. Oscillations are a signature of bad precision in the feedback and something both motifs should avoid. To complete the picture, we will focus on the noise characteristics at stable fixed points in the rest of the analysis and thus assess the control accuracy of the feedback systems for all parameter combinations.

**Noise Characteristics for Time-Delayed Feedback.** The straightforward way to study the stochastic time-delayed system is to simulate trajectories using a slightly modified Stochastic Simulation Algorithm (SSA) (16), where the delayed events lead to a state change in SSA after the delayed time (6–8). Because a simulation follows an individual trajectory, the complete state history is known and the nonmemoryless aspects of the time-delayed system is not a problem, although the stochastic process cannot be described with an explicit master equation in closed form. The convergence of the stochastic time-delayed system to a deterministic one is controlled by the volume parameter Ω, the inverse of which is proportional to a step in concentration due to a discrete molecular event (*SI Text*). Simulated stochastic trajectories (*SI Text*) confirm the deterministic bifurcation analysis in Fig. 2 in the limit of large Ω. However, for small Ω, the parameter regions where we observe oscillation are expanded due to noise-induced phase oscillation, similar to those that have been observed previously in biochemical networks (17).

The major drawback of stochastic simulations is that we only learn something about the system the for the limited number of parameter values that can be simulated. As a complement, simple mathematical expressions capturing the relevant parameter dependencies can sometimes be derived through carefully controlled approximations. One popular approximation scheme for nondelayed (Markovian) stochastic systems is the Linear Noise Approximation (LNA). The LNA is derived from an expansion in powers of $\Omega^{1/2}$ of the chemical master equation (9, 15). In a steady state, the covariance matrix in LNA is determined by the size and frequency of jumps from the stationary solution and the relaxation rate back to the same. Let $\mathbf{a}(\mathbf{x})$ be the transition rate vector and $\mathbf{S}$ the stoichiometric matrix, such that the steady state $\mathbf{x}$ is the solution of $\mathbf{Sa}(\mathbf{x}) = 0$. The relaxation rates are given by the eigenvalues of the Jacobian matrix $\mathbf{A}$ and the size and frequency of perturbations by the diffusion matrix $\mathbf{V} = \mathbf{S}\,\mathrm{diag}(\mathbf{a})\mathbf{S}^T$. The steady-state covariance matrix $\mathbf{C}$ satisfies Lyapunov's matrix equation,

$$\mathbf{AC} + \mathbf{CA}^T + \Omega\mathbf{V} = \mathbf{0}, \qquad [7]$$

which makes it possible to approximate the covariance and the noise characteristics from the steady-state solution of the system.

There are no well-established methods for estimating the stochastic properties of time-delayed chemical reaction systems. For this reason, we have developed an extension of the LNA framework to estimate the impact of time delays at stable fixed points (*SI Text*). The method depends on the conditional probability density function $p(x,y,t|\tilde{x},\tilde{y},t-\tau)$, i.e., the probability that the system is in state $x,y$ at time $t$ given that it was at $\tilde{x},\tilde{y}$ at an earlier time $t-\tau$. The delayed ODEs for the mean values are independent of $p(x,y,t|\tilde{x},\tilde{y},t-\tau)$ but additional assumptions are needed for the covariances. The conditional probability density can be approximated in two extreme cases:

1. If $x,y$ and $\tilde{x},\tilde{y}$ are independent, $p(x,y,t|\tilde{x},\tilde{y},t-\tau) = p(x,y,t)$. This is likely to be a good approximation if $\tau$ is large.
2. If $\tau$ is zero, $p(x,y,t|\tilde{x},\tilde{y},t-\tau) = \delta(x-\tilde{x})\delta(y-\tilde{y})$. The Kronecker delta function $\delta(\cdot)$ is zero everywhere except for the origin where $\delta(0) = 1$. This is a good approximation if $\tau$ is small.

Next, we assume that $p(x,y,t|\tilde{x},\tilde{y},t-\tau)$ can be expressed as a linear combination of the two extremes with a nonnegative weight $\theta(\tau)$ satisfying $\theta(0) = 0$ and $\lim_{\tau\to\infty}\theta(\tau) = 1$ such that

$$p(x,y,t|\tilde{x},\tilde{y},t-\tau) = (1-\theta)\delta(x-\tilde{x})\delta(y-\tilde{y}) + \theta p(x,y,t). \qquad [8]$$

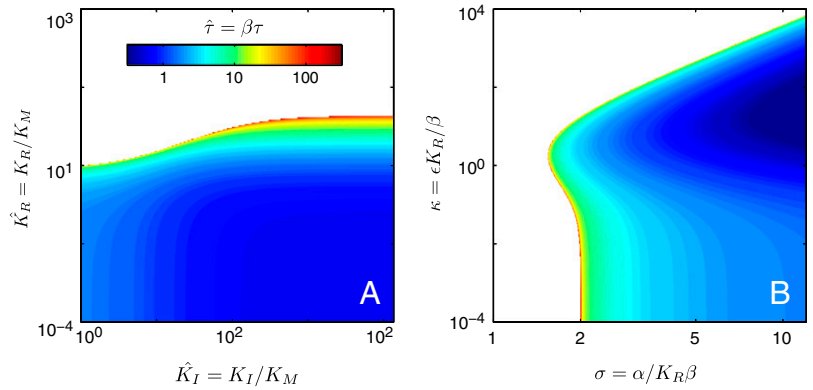


**Fig. 2.** (*A*) The bifurcation diagram of the CEA motif (with $\hat{V}_{\max} = \hat{\xi} = 10$). (*B*) The bifurcation diagram of the FCD motif. In the white areas, both motifs display stable fixed points for any delay and, in the colored regions, stable oscillations for long delays. The color corresponds to the specific delay that for this choice of parameters gives stable oscillations.

Given Eq. **8**, we can estimate the covariance matrix and all properties given by second moments, like the Fano factor and the modified Fano factor (11) (*SI Text*).

For the CEA motif, the Fano factor can be approximated by

$$\mathcal{F}_X = \frac{1+\tilde{K}_I}{T+1+\tilde{K}_I} \times \left( T + \frac{1+2\tilde{K}_I}{1+n(1-\theta)(1+\tilde{K}_I)/(1+\tilde{K}_R^n)} \right) \quad [9]$$

when $\xi \gg K_M$ (when $E_2$ is near saturation). $T = V_{\max}/(\xi\beta)$ is the turnover ratio of the product and the enzyme, and $\tilde{K}_I = K_I/\xi$ and $\tilde{K}_R = K_R/\xi$. The turnover ratio can be interpreted as how many times the $X$ pool can be turned over during the average lifetime of an enzyme.

For the FCD motif, the modified Fano factor becomes

$$\mathcal{F}_{X-Y} = \frac{\mathrm{Var}(X-Y)}{2\langle X \rangle} = \frac{\kappa x_0 + 2}{2(1+\eta(1-\theta))}, \quad [10]$$

where $x_0$ is the steady-state solution and $\eta = n(\kappa x_0 + 1)(1 - \frac{x_0(\kappa x_0+1)}{\sigma})$. The actual shape of the time-delay function $\theta(\tau)$ is unknown and an exact expression may not exist. Here we let $\theta(\tau) = 1 - e^{-k\tau}$, which fulfills the asymptotic properties implying $p(x,y,t|\tilde{x},\tilde{y},t-\tau) = p(x,y,t) + e^{-k\tau}(\delta(x-\tilde{x})\delta(y-\tilde{y}) - p(x,y,t))$ and where $k$ is a system-specific constant, reflecting the timescale of correlations in the system. In Fig. 3, we plot the Fano factor of $X$ in the CEA motif and the Fano factor of the imbalance $X-Y$ in the FCD system as functions of the time delay $\tau$. The analytical approximations in Eqs. **9** and **10** are compared with simulated noise levels.

Based on the analysis of first and second moments, we can now discuss how different feedback strengths (repression and inhibition) and product formation rates optimize the control accuracy and throughputs of the motifs. We will here assume that the system volume $\Omega$ and the time delay $\tau$ are constraints for the individual motifs and focus on finding the optimal parameters $\epsilon$, $K_R$, and $K_I$. These parameters are local in the sense that they are free to evolve without compromising the performance of other parts of the cell.

**Control Accuracy of the CEA Motif.** In controlling the enzymatic activity by a combination of direct product inhibition and delayed transcriptional feedback repression, the role of the control system is to reduce variation in the metabolite concentration. For this reason, the control systems should avoid parameter combinations that result in sustained oscillations. These parameters can be identified already in the deterministic analysis (Fig. 2 and *SI Text*). Outside the oscillatory regime, the success in suppression of intrinsic noise as described by the control accuracy $\Psi_{\mathrm{CEA}}$ can be directly calculated by the reciprocal of the Fano factor (Eq. **10**). Although the full expression is relatively simple, we will zoom in on two important limits. With $n = 2$ and a limited $k\hat{\tau}$ (no oscillations), we have

$$\Psi_{\mathrm{CEA}} \begin{cases} \geq 1 & \text{if } \tilde{K}_I \ll 1 \quad (\text{for all } T \text{ and } K_R) \\ \approx \frac{1}{T+e^{k\hat{\tau}}} & \text{if } \tilde{K}_I \gg 1 \quad \text{and} \quad \tilde{K}_R < 1 \end{cases} \quad [11]$$

The first line represents strong direct product inhibition, and the second line little or no direct feedback inhibition with strong transcriptional feedback. The control accuracy of the transcriptional feedback is thus directly related to the turnover ratio $T$ of the product and the enzyme. When the turnover ratio is high

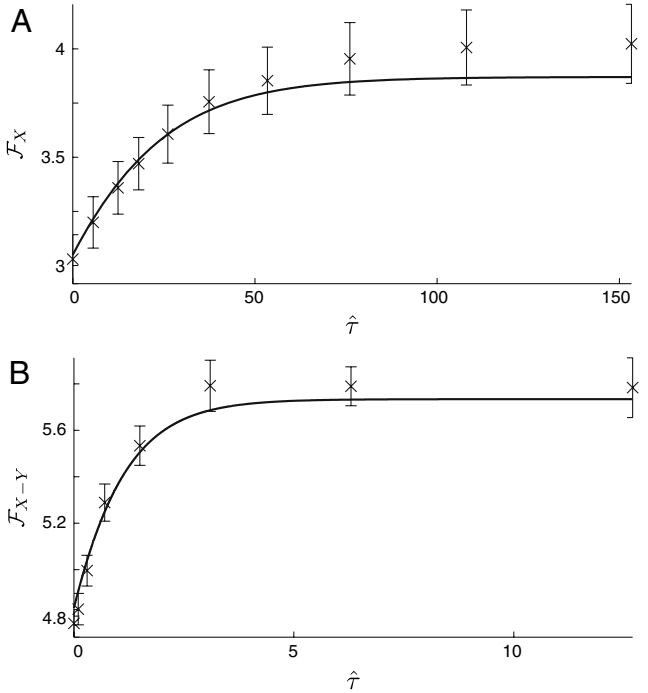


**Fig. 3.** In (*A*), the Fano factor showing the fluctuations of molecules $X$ in the CEA motif as a function of feedback delay $\tau$ when $K_I = 20$, $K_R = 40$, $V_{\max} = 1$, and $\hat{\xi} = 10$ for a size $\Omega = 1,000$. The solid line is the LNA estimation using $k = 0.05$. In (*B*), the modified Fano factor showing the imbalance of molecules for the FCD motif with $\sigma = 1$, $\kappa = 100$ and size $\Omega = 1,000$. The solid line is the LNA estimation using $k = 1$.

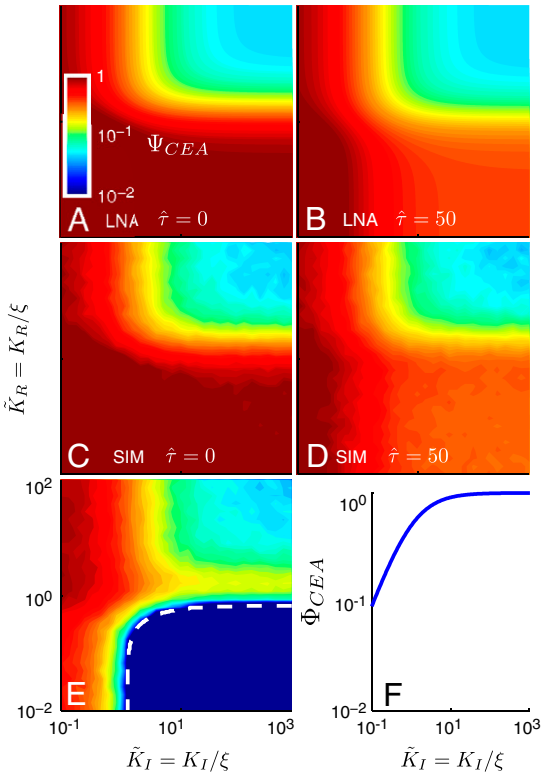


**Fig. 4.** Control accuracy of the CEA motif with a turnover ratio of $T = 0.01$ calculated using LNA, (*A*) with no time delay and (*B*) with a time delay $\tau = 50/\beta$ ($k = 0.02$). Stochastic simulation of the CEA motif with the same turnover ratio as *A* and *B*, again with no delay (*C*) and with a delay $\tau = 50/\beta$ (*D*). In (*E*), a stochastic simulation with turnover ratio $T = 1$ and delay $\tau = 1/\beta$. The dashed line shows the bifurcation separating sustained oscillations from non-oscillatory solutions in the mean-field approximation. In (*F*), the throughput is plotted as a function for increasing $K_I$ (decreasing inhibitory feedback). In the simulations, $\Omega = 1,000$ and in all panels $\hat{\xi} = 10$ and $n = 2$.

($T > 1$), the response in the transcriptional regulation which operates at a timescale $1/\beta$ is slow compared to the turnover of the $X$ pool and it loses its precision. In this situation, direct product inhibition is needed to suppress fluctuations and its contribution to the control accuracy is given by moving from the second to the first line in Eq. **11**.

On the other hand, if the turnover ratio is small ($T < 1$), the transcriptional feedback is sufficiently fast to obtain a high control accuracy and direct product inhibition will only improve the control accuracy marginally at the cost of a reduced throughput (Fig. 4*F*). If the product pool is slowly turned over ($T < 1$), direct product inhibition is therefore only useful when transcriptional feedback is delayed. In Fig. 4, we display the control accuracy $\Psi_{\mathrm{CEA}}$ (Fig. 4 *A–E*) as a function of $\tilde{K}_R$ and $\tilde{K}_I$ with and without time delay. The first row is the estimation of the control accuracy using LNA and the second row the measured control accuracy from simulations. To illustrate how accurately the modified LNA accounts for the effect of the delay, we use a low turnover ratio $T = 0.01$, and in the right column (Fig. 4 *B* and *D*) a delay $\tau = 50/\beta$.

From the deterministic bifurcation analysis (Fig. 2), we know that oscillations may occur if the delay is long enough and we have a strong transcriptional repression. This is shown in Fig. 4*E*. The dashed line is the bifurcation separating oscillating from nonoscillating solutions. Oscillations can however be avoided by either decreasing the turnover ratio, or increasing the inhibition feedback. In Fig. 4*F*, the throughput is plotted as a function of decreasing inhibition feedback (increasing $K_I$).

**Control Accuracy of the FCD Motif.** The mean-field analysis of the FCD motif revealed that the delay may cause reduced control accuracy to the point that oscillations appear resulting in unbalanced $X$ and $Y$ pools. We now move back to the original variables and discuss control accuracy in these parameters, i.e., $K_R$, the feedback strength, and $\epsilon$, the association rate. In this analysis, the flux $\alpha = 1$ and the decay $\beta = 1$ define the units for concentration and time. We calculate the control accuracy in the vicinity of a stable fixed point from the elements of the covariance matrix (*SI Text*), for $n = 2$:

$$\Psi_{\mathrm{FCD}} \approx 1 - \frac{\epsilon K_R}{4\Omega}. \qquad [12]$$

Here the time delay will not play as important a role to the increase in intrinsic noise as it did for the CEA motif. On the other hand, we do not have the same freedom in choosing parameter combinations that avoid oscillations, and therefore there will be a delicate balance in selecting the correct feedback strength to reduce noise yet avoid oscillations. The LNA holds well for volumes $\Omega > \epsilon K_R/4$. Quite surprising at first sight, the LNA predicts lower control accuracy when increasing the association rate constant $\epsilon$. To understand this, we need to consider that the same rate of product formation $\epsilon\langle XY\rangle$ can be achieved by many different combinations of $X$ and $Y$. The consumption is thus close to zero order because the flux is not changed when $X$ and $Y$ change in opposite directions, which allows for very large anticorrelated fluctuations (1, 9). If the flux is unchanged and $\epsilon$ is increased, $\langle XY\rangle$ decreases to the point where one of $X$ and $Y$ is very close to zero and the other one abundant. The control accuracy is thus very low with the result that $\langle X\rangle + \langle Y\rangle$ is much higher than with balanced pools resulting in a disproportionally high loss through the decay pathway. The direct benefits of a high association rate is thus overshadowed by the imbalanced stochastic fluctuations it renders.

From our stochastic simulations of the FCD motif in Fig. 5, we show the throughput (Fig. 5 *A–D*) and control accuracy (Fig. 5 *E–H*) as functions of $K_R$ and $\epsilon$ for two different volumes of the systems; $\Omega = 10$ in the left column and $\Omega = 10^4$ in the right column. For both control accuracy and throughput, the first row is without delay and the second row with a delay $\tau = 2$.

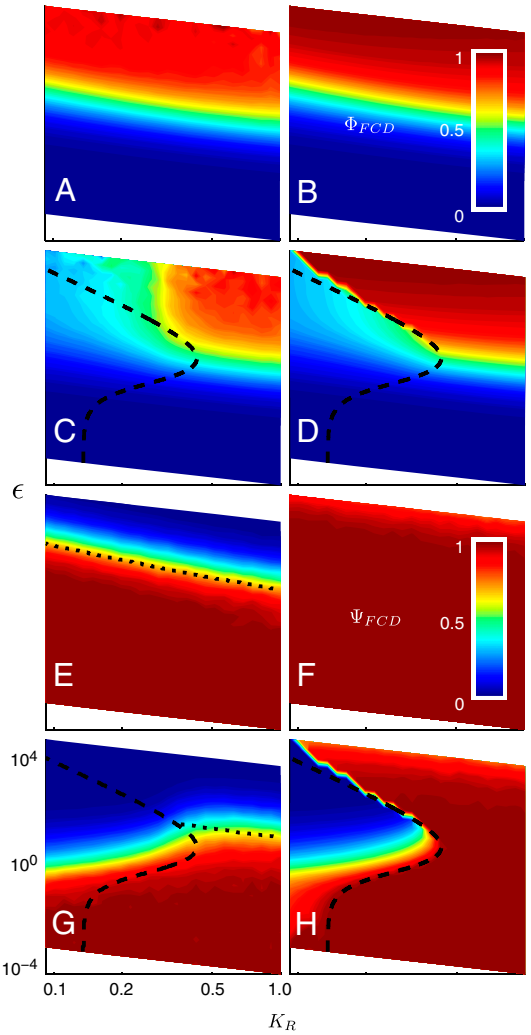


**Fig. 5.** Throughput (*A–D*) and control accuracy (*E–H*) for the FCD motif. (*Left*) We have $\Omega = 10$ and (*Right*) $\Omega = 10^4$. For both throughput and control accuracy, the upper row is without delay and the lower row is with a delay $\tau = 2$. The dashed line shows the bifurcation separating sustained oscillations from nonoscillatory solutions in the mean-field approximation and the punctuated line shows where the LNA estimates the control accuracy to be 1/2. In all panels, $n = 2$, $\alpha = 1$, and $\beta = 1$.

Without delay (Fig. 5 *A* and *B*), we see that the throughput is increased if we increase the association rate $\epsilon$, because $X$ and $Y$ pools shrink and feedback does not limit the throughput. Furthermore the control accuracy (Fig. 5 *E* and *F*) is limited by fluctuations according to Eq. **12**. Consequently, the control parameters should be in the region $\epsilon K_R < 4\Omega$. This region is more extended in large systems with high $\Omega$. The dotted line shows where the control accuracy is calculated to be 0.5 using time-delayed LNA. Increasing the feedback by reducing $K_R$ will improve control accuracy (and reduce throughput), just as predicted by the LNA.

Now if we also consider systems with delays, we can see that the control accuracy (Fig. 5 *G* and *H*) is reduced in the region where we predict oscillations. The dashed line shows the Hopf bifurcation from the mean-field analysis, i.e., where sustained oscillations appear for large $\Omega$. In contrast to when we have no delay, increasing the feedback, by decreasing $K_R$, will no longer increase the control accuracy because it will make the system move into an oscillatory state as the regulatory precision is lost

altogether. The oscillations will also decrease the throughput (Fig. 5 *C* and *D*) of the system because the synthesis systems are inhibited a significant fraction of the time.

## Discussion

Because of the stochastic nature of chemical reactions, cells have to use regulatory systems to maintain homeostasis also in a constant environment. This is particularly true for processes that should operate close to a critical point, such as the point of saturation of an enzyme or the balance point of two fluxes. Here, lack of regulation leads to suboptimal or deleterious effects due to high sensitivity accompanied by large fluctuations. We have analyzed how these systems should be optimally feedback regulated when we consider that the regulatory system responds to time-delayed signals, for instance due to the time it takes to express proteins. We find that the optimal control systems operate very differently when the time delays are considered. In particular, the optimal parameter region is much smaller for time-delayed control systems. For instance, in the choice between transcriptional regulation and direct product inhibition in the enzyme system, the nondelayed system can in many situations be accurately operated with only transcriptional regulation, whereas the time-delayed system benefits greatly from having a direct product inhibition, although this comes at the cost of maintaining a pool of inhibited enzymes. A similar tradeoff is found in the flux-coupled system, where strong nondelayed feedback can be used to balance the fluxes at a relatively low cost. Whereas, in the time-delayed system, strong feedback is not an option because it leads to oscillations. Instead the system is restricted to a small optimal region with moderate feedback and larger enzyme pools.

The analysis of these time-delayed stochastic control systems was made possible by our extension of the Linear Noise Expansion. Using this mathematical tool we can derive approximate analytical expressions for the variance and covariances of the fluctuations around stationary points in the time-delayed system that would appear identical in conventional deterministic treatment. The analytical approximations clarify the behaviors of the system over a much larger parameter space than what can be analyzed or visualized using stochastic simulations.

Based on the results for two simple regulatory motifs, we conclude that a careful examination of how time-delayed regulation and stochastic kinetics operate together will be necessary to understand the constraints for the evolution of complex intracellular control systems.

**ACKNOWLEDGMENTS.** We are grateful for helpful discussions and comments from David Sumpter. This work was supported by the European Research Council (203083), the Swedish Foundation for Strategic Research, The Knut and Alice Wallenberg Foundation, and the Swedish Research Council.

1. Paulsson J, Ehrenberg M (2001) Noise in a minimal regulatory network: plasmid copy number control. *Q Rev Biophys* 34:1–59.
2. Elf J, Nilsson D, Tenson T, Ehrenberg M (2003) Selective charging of tRNA isoacceptors explains patterns of codon usage. *Science* 300:1718–1722.
3. Ibarra RU, Edwards JS, Palsson BO (2002) *Escherichia coli* k-12 undergoes adaptive evolution to achieve in silico predicted optimal growth. *Nature* 420:186–189.
4. Shen-Orr SS, Milo R, Mangan S, Alon U (2002) Network motifs in the transcriptional regulation network of *Escherichia coli. Nat Genet* 31:64–68.
5. Novak B, Tyson JJ (2008) Design principles of biochemical oscillators. *Nat Rev Mol Cell Biol* 9:981–991.
6. Elf J, Ehrenberg M (2005) Near-critical behavior of aminoacyl-tRNA pools in *E. coli* at rate limiting supply of amino acids. *Biophys J* 88:132–146.
7. Bratsun D, Volfson D, Tsimring LS, Hasty J (2005) Delay-induced stochastic oscillations in gene regulation. *Proc Natl Acad Sci USA* 102:14593–14598.
8. Tian T, Burrage K, Burrage PM, Carletti M (2007) Stochastic delay differential equations for genetic regulatory networks. *J Comput Appl Math* 205:696–707.
9. Elf J, Paulsson J, Berg OG, Ehrenberg M (2003) Near-critical phenomena in intracellular metabolite pools. *Biophys J* 84:154–170.
10. Neidhardt FC (1996) *Escherichia coli* and Salmonella Cellular and Molecular Biology. (American Society for Microbiology, Washington, DC), 1, pp 391–600.
11. Elf J, Ehrenberg M (2003) Fast evaluation of fluctuations in biochemical networks with the linear noise approximation. *Genome Res* 13:2475–2484.
12. Levine E, Zhang Z, Kuhlman T, Hwa T (2007) Quantitative characteristics of gene regulation by small RNA. *PLoS Biol* 5(9):e229.
13. Mehta P, Goyal S, Wingreen NS (2008) A quantitative comparison of sRNA-based and protein-based gene regulation. *Mol Syst Biol* 4:221.
14. Nomura M (1999) Regulation of ribosome biosynthesis in *Escherichia coli* and *Saccharomyces cerevisiae*: Diversity and common principles. *J Bacteriol* 181:6857–6864.
15. van Kampen NG (2004) *Stochastic Processes in Physics and Chemistry* (Elsevier, Amsterdam), 5th Ed, pp 166–192 pp 244–267.
16. Gillespie DT (1976) A general method for numerically simulating the stochastic time evolution of coupled chemical reactions. *J Comput Phys* 22:403–434.
17. Vilar J, Leibler S (2002) Mechanisms of noise-resistance in genetic oscillators. *Proc Natl Acad Sci USA* 99:5988–92.